Electronic structure of 2*H*-SnSe₂: *ab initio* modeling and comparison with experiment

D.I. Bletskan, K.E. Glukhov, V.V. Frolova
Uzhgorod National University,
54, Voloshin str., 88000 Uzhgorod, Ukraine
E-mail: crystal_lab457@yahoo.com

Abstract. Energy band structure, total and local partial densities of states, spatial distribution of electronic density of 2*H*-SnSe₂ have been calculated using the density functional theory method in LDA and LDA+U approximations both with and without consideration of spin-orbit interaction. From the band structure calculation results, it follows that 2*H*-SnSe₂ is an indirect-gap semiconductor. The calculated band structure is compared with the dispersion curves $E(\mathbf{k})$ plotted using the known measurement results of angular dependent photoemission spectra. It has been observed the good agreement between theoretical and experimental dispersion curves. The calculated total and local partial densities of states have been compared with the known experimental data obtained using XPS, UPS, ARXPS, BIS methods.

1. Introduction

Tin diselenide (SnSe₂) belongs to the family of layered semiconductors with the general chemical formula of MX₂ (M – metal, X – chalcogen) [1–3]. Tin diselenide with a layered structure possesses unique physical and chemical properties that offer new opportunities for its practical application as the electrode material for lithium-ion batteries [4, 5], the memory elements on the phase change effect [6], the electric keys [7], the field-effect transistors [8], the SnS₂-SnSe₂-SnS₂ hetero-structures created by van der Waals epitaxy [9]. Physical principles for the manufacture and development of devices and equipment based on tin diselenide are related with the features of its crystal structure, electronic energy structure, and the selection rules for optical transitions. All these reasons stimulate further studying its physical properties, which is impossible without the detailed study of its electronic structure.

There is a number of theoretical works devoted to studying the electronic structure of the simplest 2*H*-polytype SnSe₂ using different calculation methods of: the empirical pseudopotential [10-14], *a priori* pseudopotential [15], parameterized and semi-empirical tight-binding method [16, 17]. Table 1 summarizes the main characteristics of 2*H*-SnSe₂ electronic spectrum obtained using the specified calculation methods. Despite acceptable qualitative reproducability of the main features of electronic structure of the 2*H*-SnSe₂ crystal in the most calculations, there are differences in the quantitative characteristics of electronic structure: the total width of the valence bands, values of the direct and indirect band gaps, sequence and topology of some energy bands, details of density of states and, most important, places of localization of the valence band top and conduction band bottom, and, consequently, transitions forming direct and indirect gaps. Thus, the results of different papers are hard to compare with each

Table 1. The main features and parameters of the 2*H*-SnSe₂ energy spectrum obtained by different calculation methods.

Calculation method	Indirect optical transitions		Direct optical transitions		References
	E_{gi}, eV	Transition type	E_{gd}, eV	Transition type	
The empirical pseudopotential method	0.81	$\Gamma_1' \rightarrow L_1'$	1.78	$M_1' \rightarrow M_2'$	[10]
The local empirical pseudopotential method	0.91	$\Gamma_1' \rightarrow L_1$	1.75	$M_2 \rightarrow M_1$	[11]
The local empirical pseudopotential method	1.10	$\Gamma_2^- \rightarrow U_1$	1.70	$M_2^+ \rightarrow M_1^+$	[13]
The *a priori* pseudopotential method	1.40	$\Gamma_4 \rightarrow M_1$	1.10	$\Gamma_4 \rightarrow \Gamma_1$	[15]
The tight binding method	1.44	$\Gamma_2^- \rightarrow L_1^+$	1.63	$\Gamma_2^- \rightarrow \Gamma_1^+$	[16]
The semi-empirical tight binding method	1.0	$M_2^+ \rightarrow \Gamma_1^+$	1.6	$M_2^+ \rightarrow M_1^+$	[17]
The density functional method DFT-LDA	0.55	$\Gamma_4 \rightarrow U_1$	0.94	$\Gamma_4 \rightarrow \Gamma_1$	Our calculation
The density functional method DFT-LDA+*U*	0.99	$\Gamma_4 \rightarrow U_1$	1.26	$\Gamma_4 \rightarrow \Gamma_1$	Our calculation

other due to the differences in the used calculation methods and because of introducing the empirical parameters. Besides, the vast majority of available 2*H*-SnSe₂ band structure calculations are performed without any consideration of the relativistic effects, and the group-theoretical analysis results presented in Refs. [10, 11] contain a number of mistakes, which was indicated by other authors [13]. The significant differences also observed in the experimental energy values of direct and indirect band gaps [18-20].

In this paper, the energy band structure as well as total and local partial densities of states of the 2*H*-SnSe₂ crystal were calculated using the density functional theory (DFT) method in the local density approximation (LDA) and in the approximation supplemented by taking into account Coulomb interaction (LDA+*U*). The character of analyzed chemical bonding is based on calculations of the spatial distribution of electronic charge density.

2. Crystal structure

2*H*-polytype SnSe₂ is characterized by the structure of brucite type based on the three-layer –Se–Sn–Se– packets ("sandwiches") that are parallel to the (001) plane. Each three-layer packet consists of a tin atoms monolayer enclosed between two close-packed monolayers of selenium atoms (Fig. 1a). The distance between three-layer packets (3.08 Å) doubly exceeds the distance between atomic monolayers within one "sandwich" (1.53 Å). In the 2*H*-SnSe₂ crystal structure, tin atoms are centered in the ideal octahedrons with the vertices on the Se atoms (Fig. 1b). The [SnSe₆] octahedra are related with each other by common edges and form the three-layer –Se–Sn–Se– packets. Chemical bonding within three-layer packets has the ion-covalent character, while chemical bonding between three-layer packets is mainly provided by van-der-Waals forces causing large anisotropy of physical properties.
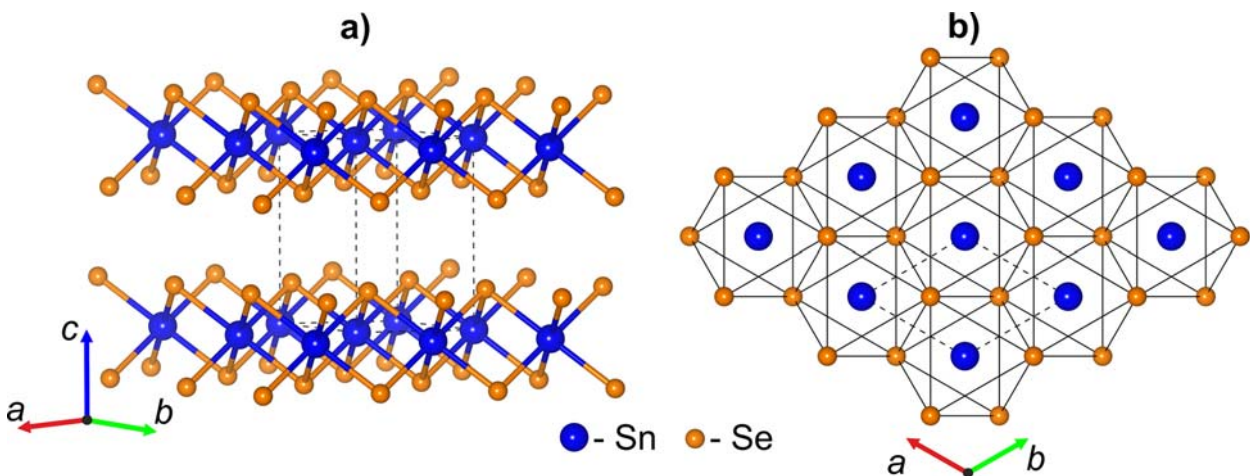

Fig. 1. Crystal structure (a) and the structure projection on XY plane with the highlighted [SnSe₆] octahedra (b) of 2*H*-SnSe₂.

In the 2*H*-SnSe$_2$ structure, an order of the layers stacking is [AγB, AγB], where γ denotes the tin atom layer, while A and B – selenium layers. The symmetry of the 2*H*-polytype crystal lattice is characterized by D_{3d}^3 ($P\bar{3}m1$) space group, and the crystalline class corresponds to the D_{3d} point group. The crystal lattice parameters are as follows: $a = b = 3.811$ Å, $c = 6.141$ Å, γ = 120° [3].

The unit cell of 2*H*-polytype contains three atoms belonging to one three-layer packet only. If the usual coordinate system is used, the unit cell is described by two vectors a_1 and a_2 in the XY plane and makes the angle 120° between them, as well as *c* vector along *Z* direction, and contains the Sn atom located in Wyckoff position $a(0, 0, 0)$ and two selenium atoms located in Wyckoff position $d(1/3, 2/3, z)$ with coordinates of (1/3, 2/3, *u*), (2/3, 1/3, *w*) where $u = 0.24920$, $w = 0.75080$. The symmetry of the specified positions is described by the local groups $\bar{3}m$ and $3m$, respectively.

3. Calculation method

In this paper, band structure calculations are performed within DFT using the basis sets of the plane waves (PW) and the linear combination of atomic orbitals (LCAO), too; norm-conserving pseudopotentials were used for the numerical realization of this computational technique by means of the ABINIT and SIESTA packages [21-24]. The electronic structure calculations were carried out in the local approximation of the Kohn–Hohenberg–Sham density functional [25, 26] using the exchange-correlation potential in the approximation of Ref. [27]. In these calculations, the following electronic configurations were used: for Sn atoms – [Kr] $5s^2 5p^2$ and for Se atoms – [Ar] $4s^2 4p^4$. The influence of core electrons was considered using the pseudopotentials in parametrization of Ref. [28].

Calculations of the density of electronic states were performed using the modified tetrahedra method [29] for integration by reciprocal space with the 8×8×5 grid for 160 special *k*-points in the irreducible part of the Brillouin zone. The basis for the 2*H*-SnSe$_2$ energy states calculation counts about 2600 plane waves and has been limited by the maximum kinetic energy $E_{cut} = 20$ Ha.

For a more precise description of the electronic spectrum, it is necessary to consider Coulomb interaction, which can be achieved using the methods based on electronic density functional theory, but taking into account interatomic Coulomb and exchange interactions in the framework of the so-called LDA+*U* approximation [30, 31]. In the calculations, there were used the values of Coulomb interaction $U = 3$ eV and exchange interaction $J = 0.3$ eV parameters.

All calculations were performed using relaxation of cell constants and atomic positions with the set of convergence criteria installed to the maximum residual stress (tension) 0.1 GPa for each component of the stress tensor and the maximum component of residual force 0.01 eV/Å. The calculation of optimized structure was performed within restrictions of fixed symmetry group.

4. Results and discussion

4.1. Band structure and density of electronic states. Energy bands of the 2*H*-SnSe$_2$ crystal at all high-symmetry points and along all corresponding directions of the Brillouin zone of the hexagonal lattice (Fig. 2) calculated by the density functional theory method without account of the spin-orbit interaction in LDA and LDA+*U* approximations are shown in Figs. 3a and 3b, respectively. The energy scale origin is aligned with the highest occupied state.

The minimum indirect band gap between the empty and occupied states calculated in the LDA approximation for 2*H*-polytype SnSe$_2$ with 16 valence electrons per unit cell has appeared equal $E_{gi} = 0.55$ eV (transition $\Gamma_4 \rightarrow U_1$). As it follows from the analysis of experimental spectra of the fundamental absorption of the SnSe$_2$ single crystals grown by a gas-phase method, the minimum gap is formed by the indirect forbidden transitions with the energy gap $E_{gi} = 0.98$ eV [18], 1.03 eV [19], 0.97 eV [20]. It is known that an *ab initio* calculations in the local density approximation in the framework of the density functional theory describe precisely the dispersion of valence bands, but always underestimate the band gap between the valence and the conduction bands. We performed the band structure calculation of SnSe$_2$ in the LDA+*U* approximation (Fig. 3b) for the agreement between the calculated and experimental data. The obtained value of the indirect gap $E_{gi} = 0.99$ eV in the LDA+*U* approximation is close to the experimental one.
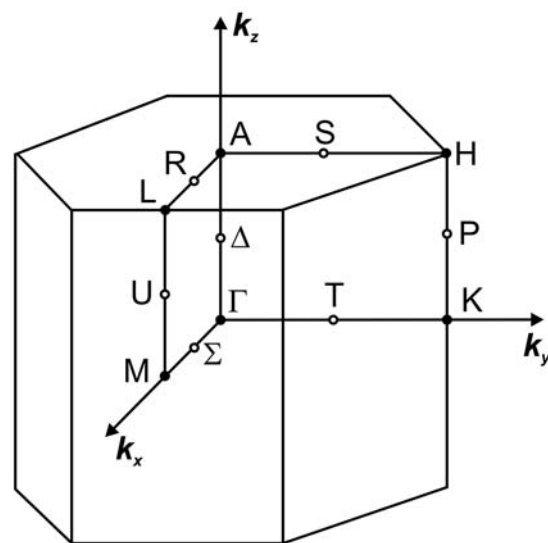

Fig. 2. Brillouin zone of hexagonal lattice. $\mathbf{k}_x$, $\mathbf{k}_y$, $\mathbf{k}_z$ – the directions of Cartesian axes in the reciprocal space.
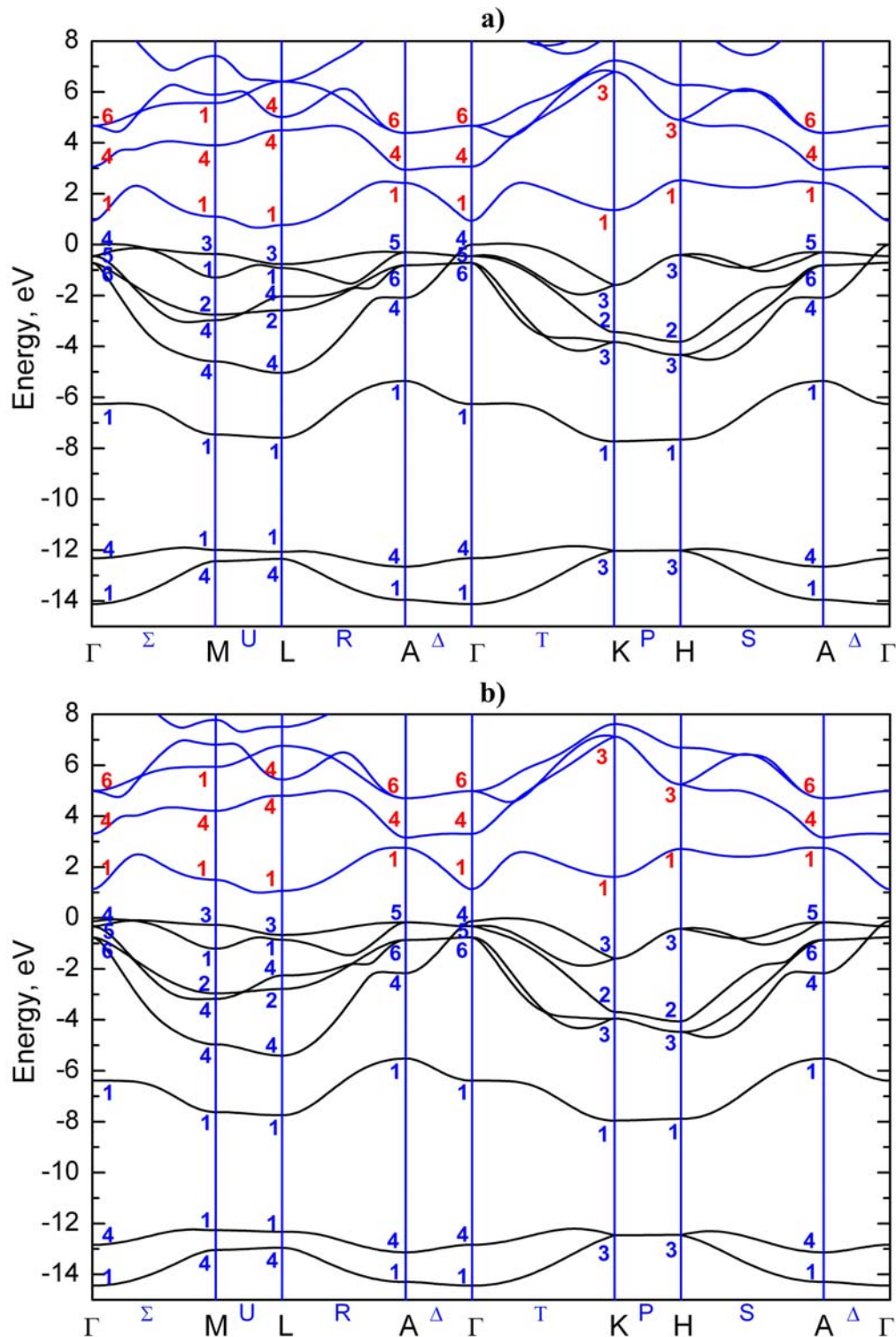
Fig. 3. Electronic structure of 2*H*-SnSe$_2$ calculated without taking into account the spin-orbit interaction in LDA (*a*) and LDA+*U* (*b*) approximations.

As for the direct transitions, there are significant differences in experimental E_{gd} values observed by different author groups. So, Evans and Hazelwood [19] indicate the existence of the indirect forbidden transitions with the energy 1.3 eV and the allowed direct transitions with the energy 1.97 eV. Two other author groups [18, 20] give the values for the allowed direct gap 2.1 eV [18] and for the forbidden direct transitions 1.62 eV [20]. From the energy band calculations in the LDA+*U* approximation, it follows that the closest to

experimental gaps are the calculated direct forbidden E'_{gd} = 1.26 eV (transition $\Gamma_4 \rightarrow \Gamma_1$) and direct allowed E''_{gd} = 2.02 eV (transition $\Gamma_6 \rightarrow \Gamma_1$) transitions.

As shown by the electronic structure calculation taking into account of the spin-orbit interaction for the 2*H*-SnSe$_2$ crystal (Fig. 4) leads to the splitting of double-degenerated states $\Gamma_6(\Delta_{so} \approx 0.08$ eV), $\Gamma_5(\Delta_{so} \approx 0.23$ eV), $A_6(\Delta_{so} \approx 0.3$ eV), $A_5(\Delta_{so} \approx 0.33$ eV), $H_3(\Delta_{so} \approx 0.1$ eV), $K_3(\Delta_{so} \approx 0.05$ eV), to the removal of degeneracy along some directions in the Brillouin zone, and it does not essentially affects the band gap value that is formed by indirect transition from the point Γ (symmetry Γ_{11}) into the point along the direction U (symmetry $\{U_3 \oplus U_4\}$), *i.e.*, it does not change the localization places of the valence band maximum and the conduction band minimum.

The layered character of the crystal is reflected in its band spectrum structure. Considerable anisotropy of dispersion law for insulated bands along and across the three-layer packets is observed. The weak dispersion $E(\mathbf{k})$ is observed along *c* axis of the crystal, *i.e.*, along the direction $\Gamma\Delta A$ that is perpendicular to the monolayers formed by Sn and Se atoms; it testifies to the layered nature of compound as well as to the relatively weak influence of interaction between the three-layer packets on the electronic structure. A significant disper-

sion of the bands along the directions parallel to the three-layer packets (Sn and Se monolayers) indicates strong interaction in the structural units [SnSe$_6$] that form the sandwiches. These features of 2*H*-SnSe$_2$ band structure allow speaking about the two-dimensional character of energy bands.

The information about contributions of atomic orbitals into 2*H*-SnSe$_2$ crystalline states can be obtained from the calculations of total and local partial densities of states. Fig. 5 shows the spectra of total $N(E)$ and local partial $n_{at}(E)$ densities of electronic states (DOS) obtained from the band calculation. Selenium 4*s*- and 4*p*-states make the main contribution to the valence band of this polytype, they are not mixed in the electronic spectrum and are separated by the forbidden energy interval. From the analysis of total and local partial densities of states for the 2*H*-SnSe$_2$ crystal, it follows that the most low-energy bunch of two valence branches located in the range from −14.14 eV to −11.87 eV below the latter occupied state is mainly created by selenium 4*s*-orbitals with an insignificant impurity of tin 5*s*- and 5*p*-orbitals. The middle divided valence subband (from −7.69 to −5.35 eV) separated from the lowest valence subband by the energy interval 4.17 eV and formed by hybridized Sn5*s*- and Se4*p*-states, which are responsible for the covalent component of chemical bonding in the [SnSe$_6$] octahedra.
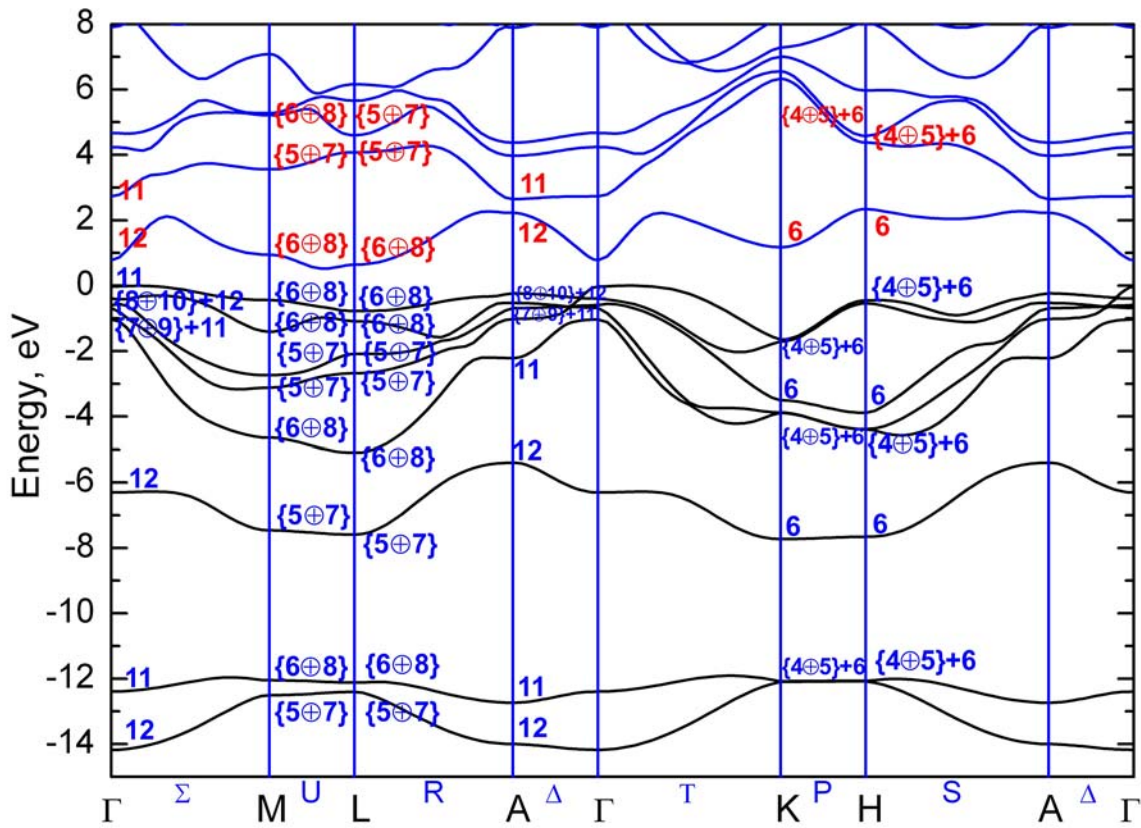

Fig. 4. Electronic structure of 2*H*-SnSe$_2$ calculated with account of the spin-orbit interaction in LDA approximation.
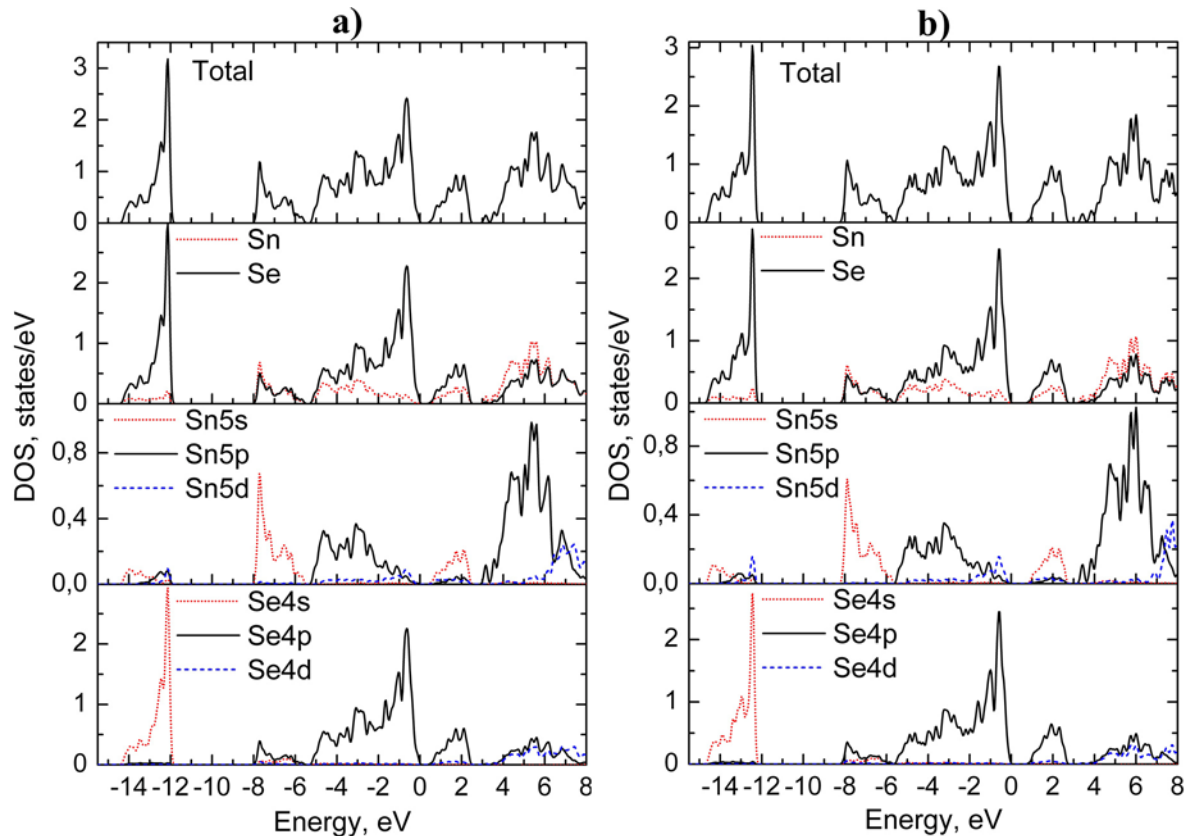
Fig. 5. Total and local partial densities of electronic states of 2*H*-SnSe$_2$ calculated in LDA (*a*) and LDA+*U* (*b*) approximations.

The upper valence subband (from –5.05 to 0 eV) is the most difficult, and it has the mixed character involving Se 4*p*-states and Sn 5*p*-states. It is virtually separated into two parts by composition: the lower part (from –5.05 to –2.0 eV) mainly formed by Se 4*p*- and Sn 5*p*-orbitals, which are responsible for the *p-p* covalent bonds Sn–Se and the upper part (from –2.0 to 0 eV) formed mainly by selenium 4*p*-orbitals, providing the weak bonds between the neighbor three-layer packets. The dominant contribution to formation of the upper part of the valence band is given by selenium 4*p*-orbitals with a negligible impurity of the virtual *d*-states of tin. The lower part of upper valence subband is formed by the bonding Se4*p*–Sn5*p*-orbitals. The characteristic feature of the 2*H*-SnSe$_2$ electronic structure is availability of forbidden interval in the conduction band, which separates the isolated low-energy unoccupied subband from the continuous spectrum of unbound states. The lowest unoccupied subband of 2*H*-SnSe$_2$ is separated from the other unoccupied subbands by the forbidden interval 0.41 eV. Hybridization of tin 5*s*-states with selenium 4*p*-orbitals is a characteristic feature of the bottom conduction band. Sn 5*s*-states are localized at the bottom of the conduction band, and further the Sn 5*p*-states are dominating with the energy increasing. The performed above analysis of the nature of crystalline orbitals in LDA approximation (Fig. 5a) remains valid

for the calculation results in LDA+*U* approximation (Fig. 5b).

4.2. Comparison of the theory and experiment. Among the number of experimental methods studying the electronic structure of layered crystals, there are the mutually complementary spectroscopic methods such as ultraviolet (UPS) and X-ray (XPS) photoelectron spectroscopy, angle-resolved ultraviolet photoelectron spectroscopy (ARPES), angle-resolved X-ray photo-electron spectroscopy (ARXPS) and bremsstrahlung isochromatic spectroscopy (BIS). The surface state of studied crystals is very important for the photoemission studies because the thickness of an analyzed surface layer is very small and amounts to tens angstroms [32]. At such low values of electrons escape depth, it is necessary to prepare ultrapure surface for obtaining reliable information from measurements of these photoelectron spectra. The special studies performed using the methods of diffraction of slow electrons and Auger spectroscopy showed that basic (001) surfaces of SnSe$_2$ layered crystals obtained by the cleavage in ultrahigh vacuum possessed the exceptional inertness in relation to the absorption of gasses [33].

4.2.1. Comparison of the calculated total density of states with X-ray and ultraviolet photoelectron spectra. The electronic states of valence band can be experimentally studied using X-ray and ultraviolet

photoelectron spectroscopies. Fig. 6 shows UPS [34, 35] and XPS [36, 37] spectra of $2H$-SnSe$_2$ crystal combined in a single energy scale with the calculated spectra of the total density of states $N(E)$ in LDA and LDA+U approximations. The valence band top is taken as the zero energy position. The shape of overall valence band spectra depends on contribution of electronic states of different orbital symmetry as well as on their photo-ionization cross-section (at a given excitation energy) for atoms of chemical elements belonging to the compound. The photoionization cross-section of electron excitation from the valence band into the vacuum depends on the symmetry of electron wave functions and on the energy of exciting quantum [38]. It is this fact, *i.e.*, the dependence of photoionization cross-section of electrons at the emission into vacuum on the energy of the exciting quantum is the main reason that the shape of valence band photoelectron spectra depends on the excitation energy (compare XPS and UPS curves). Since the photoionization cross-section of selenium $4p$-electrons exceeds the photoionization cross-section of tin p- and d-states, the main part of photoelectron spectra in the energy range from –5 to 0 eV is formed by selenium $4p$-states. It can be conditionally separated by three subbands A, B and C within this energy range (Fig. 6), which genetic origin is clearly visible when studying the polarized XPS spectra (Fig. 8).

4.2.2. Comparison of the calculated and experimental band structures. We have discussed above the photoelectron XPS and UPS spectra, in which only the energy of emitted electrons was fixed. These characteristics make it possible to define only some average characteristics of the occupied bands. In the case of angle-resolved photoemission spectroscopy (ARPES) [32], there performed are the measurements of not only the kinetic energy of photoelectron but also its distribution direction that is defined by polar and azimuthal angles, which allows finding out the complete spectrum of elementary excitations, *i.e.*, the magnitude $E(\mathbf{k})$. Really, under these conditions the experimenter automatically establishes not only the magnitude of impulse of emitted photoelectron $\mathbf{K}_i$, since $E_{kin} = \hbar^2\mathbf{K}^2/2m$, but also its direction. Photoelectron emission with angular resolution allows finding the dispersion law $E(\mathbf{k})$ by tracing the energy of spectral peaks depending on the components of the electron wave vector parallel to the crystal (001) surface of $\mathbf{k}_{||}$. Therefore, the results obtained using the method of ultraviolet photoelectron spectroscopy with angular resolution are quite enough for comparison with theoretically calculated electronic spectrum. This is especially justified in the case of $2H$-SnSe$_2$ layered crystals that have weak dispersion in one of the directions.

For the first time, the angular dependence of electron photoemission spectra from the (001) surface of SnSe$_2$ single crystals with the exciting photon energy 21.2 eV (He I) was studied in Ref. [36]. However, usage of synchrotron radiation (high intensity, total polariza-

tion, continuous spectrum) for the excitation of electrons allows to more accurately determine the electron level positions, which is very important for comparison of experimental results with the band structure calculations. The angular dependence of electron photoemission spectra of $2H$-SnSe$_2$ layered crystals at excitation by synchrotron radiation was studied in two modes [40]: 1) the changing of polar angle within the range from $\theta = -10°$ up to $\theta = 67.5°$ relatively to the normal of (001) surface at the constant energy of incident photons $h\nu = 21$ eV; 2) the changing of an incident photon energy within the range from $h\nu = 19$ eV up to $h\nu = 24$ eV at the constant polar angle $\theta = 45°$.

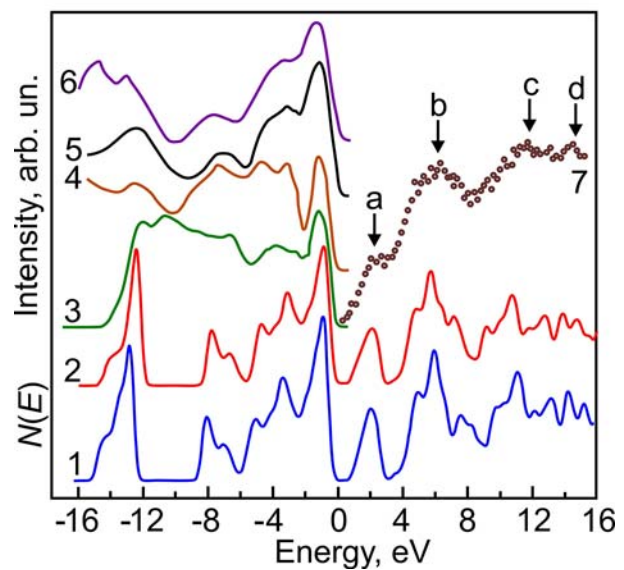**Fig. 6.** *1, 2* – theoretical calculated smoothed total density of states of $2H$-SnSe$_2$ in LDA+U and LDA; *3* – HeI UPS $h\nu = 21.2$ eV [34]; *4* – HeII UPS $h\nu = 23.09$ eV [35]; *5* – XPS $h\nu = 1486$ eV [36]; *6* – XPS $h\nu = 1486$ eV [37]; *7* – BIS $h\nu = 1486.6$ eV [39].
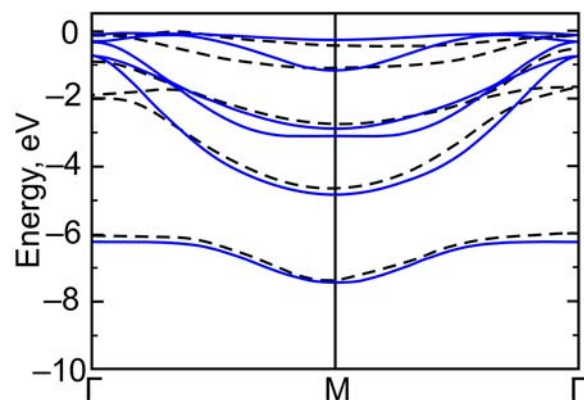

Fig. 7. Experimental (dashed lines) [40] and calculated LDA+U (solid lines) dispersion curves $E(\mathbf{k}_{||})$ of $2H$-SnSe$_2$ along the direction Γ–M–Γ of Brillouin zone.
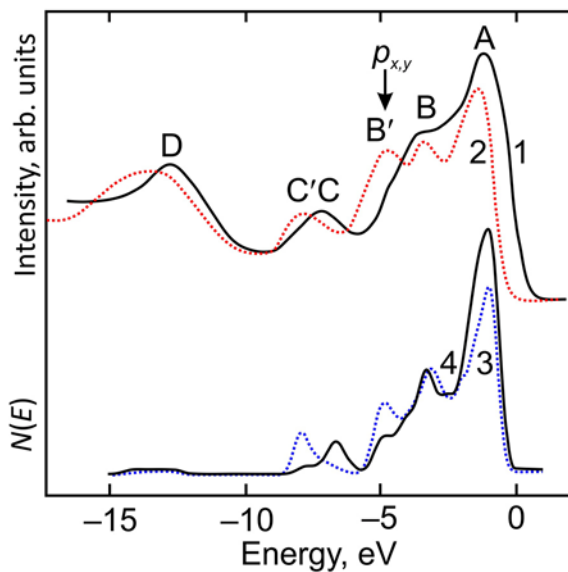
Fig. 8. XPS spectra (θ = 22°(*1*), 82°(*2*)) [41] and the calculated partial density of selenium $p_{x,y}$- (*3*), p_z-states (*4*) of 2*H*-SnSe$_2$.

The obtained data of peak positions in the spectrum as a function of the polar angle θ was used by authors of the work [40] for the construction of dispersion curves of six upper valence bands of 2*H*-SnSe$_2$ in the direction Γ–M–Γ of Brillouin zone, which we compared with the calculation results of $E(\mathbf{k})$ by density functional method (Fig. 7). The radiation energy 21 eV was insufficient to examine the two lowest valence branches located at 12...15 eV below the valence band top. Usage of polarized synchrotron excitation radiation showed the weak dispersion of peaks in 2*H*-SnSe$_2$ energy distribution curves of normal emission relatively to the changes in the photon energy, which indicates weak interlayer interaction in tin diselenide.

In contrast to ARPES with the low excitation energy ($h\nu$ = 21 eV) where the angular dependence of photoelectron spectra is mainly associated with the dispersion of energy bands, the angle-resolved X-ray photoelectron spectroscopy (ARXPS) method with the excitation photon energy $h\nu$ =1500 eV allows to directly study spatial symmetry of the structure of valence bands [41]. The photoelectron spectra of valence states of 2*H*-SnSe$_2$ layered crystals measured at the excitation by X-ray radiation with the photon energy $h\nu$ = 1500 eV for two values of the polar angles θ = 22° and 82° taken from Ref. [41] are combined in Fig. 8 in a single energy scale with our calculated local partial selenium $p_{x,y}$- and p_z-states of tin diselenide. As seen from this figure, the agreement between the calculated and experimental results is satisfactory for all bands except that the bands of experimental spectrum are more broadened. There observed are six distinct maxima in XPS spectrum in the energy range from 0 to 16 eV below the valence band top (Fig. 8, curves *1*, *2*). The intensive wide peak D at the valence band bottom is mainly caused by selenium

4*s*-electrons, while at the valence band top (A, B and B′ maxima), where selenium and tin *p*-electrons are localized, contribution of the former ones into the photoelectron spectrum is dominating. The intensities of separated bands in the spectra are redistributed with changing the electron emission angle; it allows to analyze the energy distribution of Se 4*p*-states with the different spatial symmetry. So, the density of Se 4*p*-states reaches the maximum value (peak A) within the energy range from 0 to –2 eV, the density of p_z-states are higher than that of $p_{x,y}$-states, and the valence band top of 2*H*-SnSe$_2$ in the Γ point (symmetry Γ_4) is formed by p_z-states. The $p_{x,y}$-orbitals lie in the basal plane and they are responsible for formation of peaks B′ and C′.

4.2.3. Comparison of the calculated density of states with BIS spectrum. Among X-ray spectroscopic methods, the bremsstrahlung isochromatic spectroscopy method [39] is very informative for studying the conduction band structure of tin diselenide. The bremsstrahlung isochromatic spectrum measured on the surface (001) cleaved in ultrahigh vacuum at the energy quanta 1486.6 eV is shown in Fig. 6 (curve *7*). The BIS spectra contain four maxima which nature can be identified by comparison with the calculated total and partial densities of states of conduction band (Fig. 5). So, the peak *a* is mainly formed by unoccupied selenium *p*-states with an admixture of tin *s*- and *p*-states; free tin *p*-states and selenium *p*- and *d*-orbitals make the main contribution into the peak *b*; the nature of the following two peaks *c* and *d* is similar, and it is formed by identical contribution of anion and cation *p*-, *d*-states, however, the total selenium contribution about twice exceeds the tin contribution.

4.3. Spatial distribution of electronic density. The properties of material are determined by the spatial and energy electronic structures. At the same time, the electronic structure of valence electrons represents the particular interest, and it characteristically changes at occurrence of the chemical bond between atoms. It is necessary to know the overall picture of spatial distribution of electronic density for the exact descript-tion of chemical bonding in 2*H*-SnSe$_2$ layered crystals [42]. We performed the self-consistent calculations of 2*H*-SnSe$_2$ electronic density $\rho(r)$ including hybridization effects between all atoms in four planes: (110) and $(1\bar{1}0)$ located perpendicular to the three-layer packets; (001) through tin and selenium monolayers (Fig. 9). The solid lines on contour maps describe the surfaces of constant electronic density, and the density of lines in the figures describes the gradient of electronic density.

It is seen from Figs. 9a, 9b that the electronic density is much higher within the three-layer packet (sand-wich) than at its border, which reflects the chemical bonding of tin atoms with the nearest neighbors in [SnSe$_6$] octahedron. The analysis of total electronic density distribution maps shows that the electronic density distribution in 2*H*-SnSe$_2$ layered crystal is aniso-tropic due to the difference of the nature of interatomic

interactions having the combined character and includes covalent, ionic and van-der-Waals components. As can be seen from Fig. 9a, the primary charge is concentrated on the anions (Se) and the minimum charge – in the interlayer van-der-Waals space. At the same time, it is observed the polarization of an electronic cloud in the direction from Se atom to Sn atom. The covalent component of chemical bond in the three-layer packets is reflected by the strongly pronounced deformation of ρ(*r*) contours from selenium atoms toward tin atoms along the Sn–Se bond line as well as by the presence of overall contours that cover the electronic density maxima on the cation-anion bonds. The presence of covalent component in 2*H*-SnSe$_2$ is caused by hybridization of selenium

4*p*-states and tin 5*s*-, 5*p*-states (Fig. 5). Exactly, the charge of covalent bond is responsible for stability of [SnSe$_6$] octahedral structural formations in this polytype. The ionic component is determined by the partial transfer of charge density from tin atoms to more electronegative selenium atoms. It reflects on the electronic density maps by the higher density of valence electrons near the localization places of selenium atoms and by the charge reduction in the covalent bond between selenium and tin atoms. The analysis of calculations also shows that the proportion of covalent interatomic bond in the three-layer packets is greater than the ionic because contribution of the *s*-partial density is less than *p*-component.
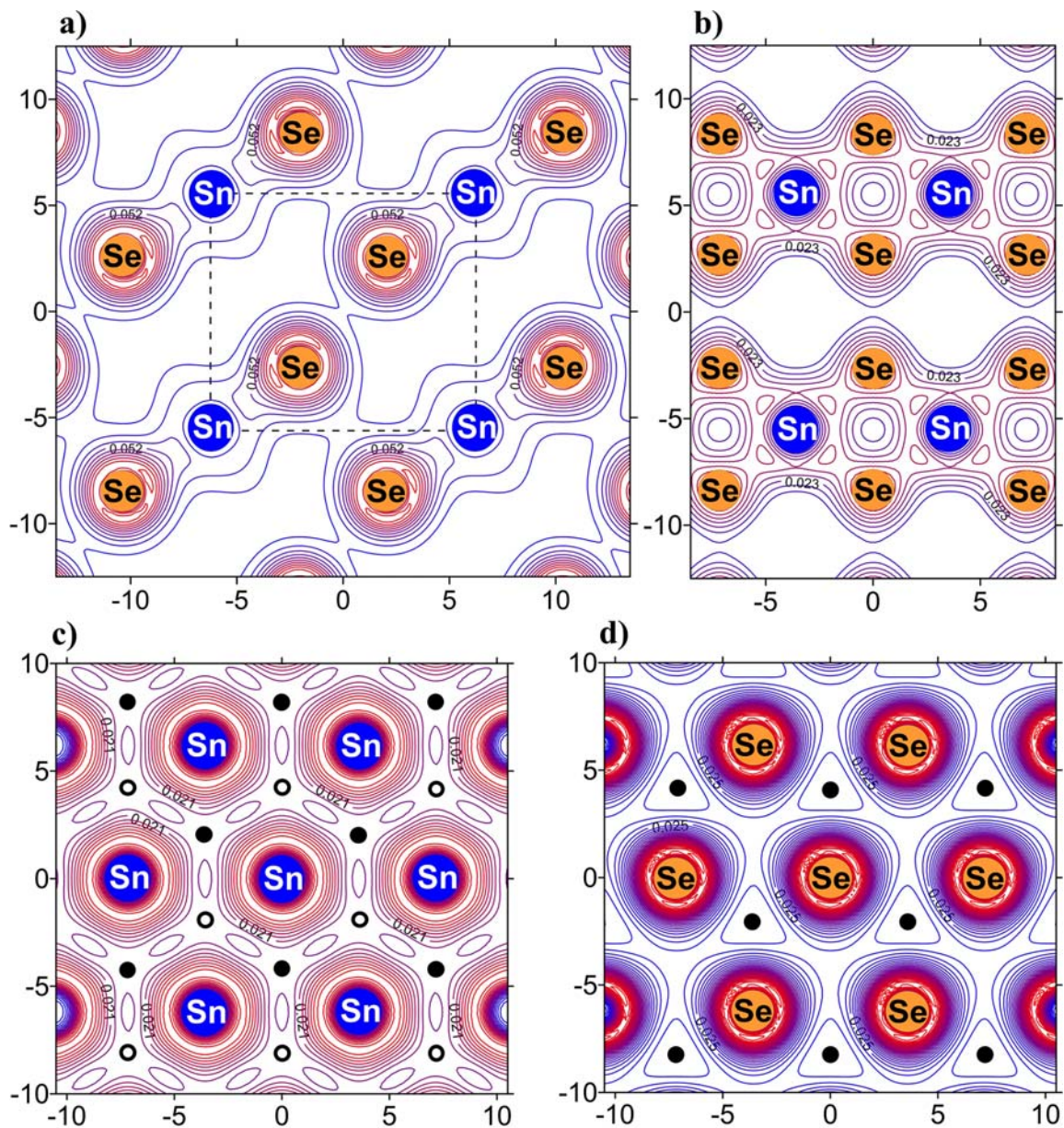

Fig. 9. Maps of total electronic density distribution for 2*H*-SnSe$_2$ crystal in (110) (*a*), ($1\overline{1}0$) (*b*), (001) of cation (*c*) (points and circles mark the locations of Se ions being in two different anion monolayers of a three-layer packet) and anion (*d*) planes.

The maps in Figs. 9c, 9d show the electron charge distribution between different selenium (tin) atoms belonging to one anion (cation) monolayer in the three-layer packet. It is seen that no overall lines for the $\rho(r)$ level for neighboring anions (cations) in monoatomic layers of selenium (tin) are observed, which testifies to the weak overlapping of their wave functions. The charge distribution in one three-layer packet forms the almost closed shell that indicates weak interpacket interaction caused by selenium p_z-states that partially enter into the interlayer space. From the density distribution contours of valence electrons presented in Fig. 9, anisotropy of electrical, optical and mechanical properties of tin diselenide layered crystals becomes understandable.

5. Conclusions

The detailed study of the 2*H*-polytype SnSe$_2$ electronic structure has been performed including calculations of the band structure with and without account of spin-orbit interaction, total and local partial densities of states as well as spatial distribution of electronic density. The calculated 2*H*-SnSe$_2$ band structure has been compared with the known dispersion curves $E(\mathbf{k})$ constructed by the measurement results of angle-dependent photo-emission spectra. A good agreement between the theoretical and experimental dispersion curves is observed, especially in the range of the top subbands of the valence band. The total density of states $N(E)$ calculated in the whole Brillouin zone for the valence band is compared with the known experimental X-ray and ultraviolet photoelectron spectra as well as for the conduction band – with the bremsstrahlung isochromatic spectra. It has been shown that the band positions and its nature in 2*H*-SnSe$_2$ electronic energy spectrum in the LDA+*U* approximation agree well with the data of photoelectron spectroscopy, which confirms the correctness of the chosen exchange and correlation parameters.

References

1. D.I. Bletskan, *Crystalline and Glassy Chalcogenides of Si, Ge, Sn and Alloys on their Base.* Zakarpattia, Uzhhorod, 2004.
2. B. Palosz, S. Gierlotka, F. Levy, Polytypism of SnSe$_2$ crystals grown by chemical transport: structures of six large-period polytypes of SnSe$_2$ // *Acta Cryst. C*, **41**(10), p. 1404-1406 (1985).
3. B. Palosz, E. Salje, Lattice parameters and spontaneous strain in AX$_2$ polytypes: CdI$_2$, PbI$_2$, SnS$_2$ and SnSe$_2$ // *J. Appl. Crystallogr.* **22**(6), p. 622-623 (1989).
4. J. Yamaki, A. Yamaji, Layered materials for lithium secondary batteries // *Physica B*, **105**(1), p. 466-470 (1981).
5. J. Choi, J. Jin, I.G. Jung et al., SnSe$_2$ nanoplate–grapheme composites as anode materials for lithium ion batteries // *Chem. Communs.* **47**(18), p. 5241-5243 (2011).
6. K.M. Chung, D. Wamwangi, M. Woda, M. Wuttig, W. Bensch, Investigation of SnSe, SnSe$_2$, and Sn$_2$Se$_3$ alloys for phase change memory applications // *J. Appl. Phys.* **103**(8), p. 083523–083523-7 (2008).
7. D. Chun, R.M. Walser, R.W. Bene, T.H. Courtney, Polarity-dependent memory switching in devices with SnSe and SnSe$_2$ crystals // *Appl. Phys. Lett.* **24**(10), p. 479-481 (1974).
8. T.S. Pan, D. De, J. Mamongo, A.M. Guloy, V.G. Hadjiev, Y. Lin, H.B. Peng, Field effect transistors with layered two-dimensional SnS$_{2-x}$Se$_x$ conduction channels: Effect of selenium substitution // *Appl. Phys. Lett.* **103**(9), p.093108-1–5 (2013).
9. R. Schlaf, C. Pettenkofer, W. Jaegermann, Band lineup of a SnS$_2$/SnSe$_2$/SnS$_2$ semiconductor quantum well structure prepared by van der Waals epitaxy // *J. Appl. Phys.*, **85**(9), p. 6550-6556 (1999).
10. M. Au-Yang, M.L. Cohen, Electronic structure and optical properties of SnS$_2$ and SnSe$_2$ // *Phys. Rev. B*, **178**(3), p. 1279-1283 (1969).
11. C.Y. Fong, M.L. Cohen, Electronic energy-band structure of SnS$_2$ and SnSe$_2$ // *Phys. Rev. B*, **5**(8), p. 3095-3101 (1972).
12. C.Y. Fong, M.L. Cohen, Electronic charge densities for layer semiconductors: SnS$_2$ and SnSe$_2$ // *J. Phys. C*, **7**(1), p. 107-112 (1974).
13. I.Ch. Schlüter, M. Schlüter, The electronic structure of SnS$_2$ and SnSe$_2$ // *phys. status solidi (b)*, **57**(1), p. 145-155 (1973).
14. M. Schlüter, M.L. Cohen, Valence-band density of states and chemical bonding for several non-transition-metal layer compounds: SnSe$_2$, PbI$_2$, BiI$_3$ and GaSe // *Phys. Rev. B*, **14**(2), p. 424-431 (1976).
15. F. Aymerich, F. Meloni, G. Mula, Pseudopotential band structure of solid solutions SnS$_x$Se$_{2-x}$ // *Solid State Communs.* **12**(2), p.139-141 (1973).
16. J. Robertson, Electronic structure of SnS$_2$, SnSe$_2$, CdI$_2$ and PbI$_2$ // *J. Phys. C: Solid State Phys.* **12**(22), p. 4753-4766 (1979).
17. R.B. Murray, R.H. Williams, Band structure and photoemission studies of SnS$_2$ and SnSe$_2$: II. Theoretical // *J. Phys. C: Solid State Phys.* **6**(24), p. 3643-3651 (1973).
18. A.K. Garg, O.P. Agnihotri, A.K. Jain, Optical absorption spectrum of tin diselenide single crystals // *J. Appl. Phys.* **47**(3), p. 997-100 (1976).
19. B.L. Evans, R.A. Hazelwood, Optical and electrical properties of SnSe$_2$ // *Brit. J. Appl. Phys.* **2**(2), p. 1507-1516 (1969).
20. G. Domingo, R.S. Itoga, C.R. Kannewurf, Fundamental optical absorption in SnS$_2$ and SnSe$_2$ // *Phys. Rev. B*, **143**(2), p. 536-541 (1966).
21. http://www.abinit.org
22. X. Gonze, B. Amadon, P.-M. Anglade *et al.*, ABINIT: First-principles approach to material and nanosystem properties // *Comput. Phys. Communs.* **180**(12), p. 2582-2615 (2009).

23. http://departments.icmab.es/leem/siesta/

24. J.M. Soler, E. Artacho, J.D. Gale, A. Garcia, J. Junquera, P. Ordejon, D. Sanchez-Portal, The SIESTA method for *ab initio* order-N materials simulation // *J. Phys.: Condens. Matter*, **14**(11), p. 2745-2779 (2002).

25. P. Hohenberg, W. Kohn, Inhomogeneous electron gas // *Phys. Rev.* **136**(3), p. B864-B871 (1964).

26. W. Kohn, L.J. Sham, Self-consistent equations including exchange and correlation effects // *Phys. Rev.* **140**(4), p. A1133-A1138 (1965).

27. D.M. Ceperley, B.J. Alder, Ground state of the electron gas by a stochastic method // *Phys. Rev. Lett.* **45**(7), p. 566-569 (1980).

28. C. Hartwigsen, S. Goedecker, J. Hutter, Relativistic separable dual-space Gaussian pseudo-potentials from H to Rn // *Phys. Rev. B*, **58**(7), p. 3641-3662 (1998).

29. P.E. Blöchl, O. Jepsen, O.K. Andersen, Improved tetrahedron method for Brillouin-zone integrations // *Phys. Rev. B*, **49**(23), p. 16223-16233 (1994).

30. V.I. Anisimov, J. Zaanen, O.K. Andersen, Band theory and Mott insulators: Hubbard U instead of Stoner I // *Phys. Rev. B*, **44**(3), p. 943-954 (1991).

31. V.I. Anisimov, F. Aryasetiawan, A.I. Lichtenstein, First-principal calculations of the electronic structure and spectra of strongly correlated systems: the LDA+*U* method // *J. Phys.: Condens. Matter*, **9**(4), p. 767-808 (1997).

32. P.Y. Yu, M. Cardona, *Fundamentals of Semiconductors: Physics and Materials Properties*, 4th ed. Springer-Verlag, Berlin Heidelberg, 2010.

33. R.H. Williams, R.B. Murray, D.W. Govan, J.M. Thomas, E.I. Evans, Band structure and photoemission studies of SnS_2 and $SnSe_2$. I. Experimental // *J. Phys. C.: Solid State Phys.* **6**(24), p. 3631-3642 (1973).

34. C.A. Formstone, E.T. FitzGerald, J.S. Foord, P.A. Cox, Photoelectron spectroscopy of silver deposition onto the van der Waals faces of $SnS_{2-x}Se_x$ crystals // *Surf. Sci.* **238**(1–3), p. 199-214 (1990).

35. C.A. Formstone, E.T. FitzGerald, P.A. Cox, D. O'Hare, Photoelectron spectroscopy of the tin dichalcogenides $SnS_{2-x}Se_x$ intercalated with cobaltocene // *Inorg. Chem.* **29**(19), p. 3860-3866 (1990).

36. R.H. Williams, A.W. Parke, The band structure of $SnSe_2$ by angle-resolved photoelectron spectroscopy // *J. Phys. C.: Solid State Phys.* **11**(12), p. 2549-2559 (1978).

37. R.B. Murray, R.H. Williams, Band structure and photoemission studies of SnS_2 and $SnSe_2$: II. Theoretical // *J. Phys. C: Solid State Phys.* **6**(24), p. 3643-3651 (1973).

38. J.J. Yeh, *Atomic Calculation of Photoionization Cross-section and Asymmetry Parameters*. Gordon and Breach Science Publisher, Amsterdam, 1993.

39. Y. Gao, B. Smandek, T.J. Wagener, J.H. Weaver, F. Lévy, G. Margaritondo, Bremsstrahlung-isochromat studies of conduction-band states in SnS_2 and $SnSe_2$ // *Phys. Rev. B*, **35**(17), p. 9357-9359 (1987).

40. Y. Bertrand, F. Solal, F. Levy, Experimental band structure of 2*H*-$SnSe_2$ by synchrotron radiation photoemission spectroscopy // *J. Phys. C: Solid State Phys.* **17**(16), p. 2879-2888 (1984).

41. L. Ley, R.H. Williams, P.C. Kemeny, Spatial symmetries of valence band structures by angularly resolved X-ray photoelectron spectroscopy // *Nuovo Cimento B*, **39**(2), p.715-719 (1977).

42. M.L. Cohen, Electronic charge densities in semiconductors // *Science*, **179**(4079), p. 1189-1195 (1973).